COMBINED FORCED AND FREE CONVECTION IN A CURVED DUCT

By

Clement G. Yam and Harry A. Dwyer

University of California, Davis

Department of Mechanical and Aeronautical Engineering

Davis, CA 95616

Abstract

The purpose of this study is to investigate the flow and heat transfer characteristics of a combined forced and free convection flow in a curved duct. Solutions are obtained by solving the low Mach number model of the Navier-Stokes equation using a control volume method. The finite-volume method has been developed with the use of a predictor-corrector numerical scheme and some new variations of the classical projection method. Solutions indicated that the existence of buoyancy force has changed the entire flow structure inside a curved duct. Reversed flow at both inner and outer bend is observed. For moderate Reynolds number the upstream section of the duct has been significantly influenced by the free convection processes. In general heat transfer is strong at the inner bend of the beginning of the heated section and at the outer bend on the last half of the heated section. The maximum velocity location is strongly influence by the combined effects of buoyancy and centrifugal forces. Strong buoyancy force can reduce the strength of the secondary flow where it plays an important role in mixing.

1) Introduction

Steady flow in a curved duct is of practical engineering interest and was first investigated by Dean [1], [2]. The main concern of the fluid mechanics problem is to determine the total pressure drop in the flow since a duct with a bend has a higher pressure drop due to the secondary motion of the fluid. Interest also occurs in this type of flow for the mixing of chemicals by the secondary motion. If the mixing is adequate, then additional pumping is not required.

Combined forced and free convection is of great importance in the design of heat exchangers like the cooling of electronic equipment by Freon-12 where inside the cooling coil the buoyancy force is higher than convection force. Moreover, the effect of secondary flow is of great important as it can enhance the overall heat transfer rate like design of a cooling coil inside a nuclear reactor. Unlike the straight duct flow, which can be solved analytically by using the parallel flow assumption, the flow in the curved section is not parallel and is more complex. Most of the recent research efforts by Masiliyah [3], Soh and Berger [4], [5], and Yao and Berger [6], are limited only to a curved duct because the problem can be written in a toroidal coordinate system. This is the first three dimensional numerical study of a curved duct with straight duct(s) attached where the usage of a non-orthogonal mesh is required.

Numerical solutions are obtained by solving the governing equations in a body fitted, non-orthogonal, coordinate system. A control volume form of the governing equations is used in this study due to clear physical interpretation of the integral equations. A detail discussion of the initial and boundary conditions for this problem is also included. Solutions are presented in the form of two-dimensional contours and three-dimensional surface contours in order to indicate the local variations. One-dimensional plots are used to show the global results. A detail discussion of the flow structure and local heat transfer rate of the combined forced and free convection flow field and its different with a forced convection flow field is also present in this study.

2) Governing Equation:

For internal flow, the dimensionless variables are defined as follows:

$$\overline{\rho} = \frac{\rho}{\rho_{inlet}}; \quad \overline{x} = \frac{x}{L}; \quad \overline{\vec{V}} = \frac{\vec{V}}{U_{ref}}; \quad \overline{P} = \frac{P - P_{ref}}{\rho_{inlet} U^2_{ref}};$$

$$\overline{T} = \frac{T - T_{inlet}}{T_H - T_{inlet}}; \quad \overline{t} = \frac{t\, U_{ref}}{L}$$

where ρ_{inlet} is the density at the inlet of the duct, L is the reference length and is the radius of the duct, T_{inlet} is the temperature of the inlet fluid, T_H is the maximum temperature of the system, t is time, U_{ref} is the reference velocity scale and is defined by the mean velocity at the inlet which has the following form:

$$U_{ref} = \frac{\iint_{\mathcal{A}} \vec{V}_{inlet} \cdot \vec{n}\, dA_{inlet}}{\iint_{\mathcal{A}} dA_{inlet}}$$

The resulting dimensionless governing equations (omitting over bars) with the Boussinesq approximation have the following forms:

1) Continuity Equation:

$$\frac{\partial}{\partial t} \iiint_{\mathcal{V}} \rho dV + \iint_{\mathcal{A}} \rho \vec{V} \cdot \vec{n}\, dA = 0$$

where t is the time, ρ is the density, $\vec{V}$ is the velocity vector, $\vec{n}$ is the unit normal vector pointing out of the control volume, dV is the finite volume, and dA is the area on each surface of the finite volume.

2) Momentum Equation:

$$\rho\frac{\partial}{\partial t}\iiint_{\nu}\vec{\nabla}\,dV+\rho\iiint_{\nu}(\vec{\nabla}\bullet\vec{\nabla})\vec{\nabla}dV$$
$$=-\iint_{\mathcal{A}}P\vec{n}\,dA+\frac{1}{Re}\iint_{\mathcal{A}}\bar{\bar{\tau}}\bullet\vec{n}\,dA-\frac{Ra}{Re^2\,Pr}\iiint_{\nu}\rho T\,dV$$

3) Thermal Energy Equation:

$$\frac{\partial}{\partial t}\iiint_{\nu}T\,dV+\iiint_{\nu}(\vec{\nabla}\bullet\vec{\nabla})\,T dV$$
$$=\iint_{\mathcal{A}}\vec{\nabla}T\bullet\vec{n}\,dA+Ec\,Pr\iiint_{\nu}\phi\,dV+Ec\left(\frac{\partial}{\partial t}\iiint_{\nu}\rho P\,dV\right.$$
$$\left.+\iint_{\mathcal{A}}\rho P\vec{\nabla}\bullet\vec{n}\,dA\right)$$

where Rayleigh Number (Ra) $=\dfrac{g\beta L^3\Delta T}{\nu\alpha}=\dfrac{\text{Buoyancy Force}}{\text{Viscous Force}}$

Prandtl Number (Pr) $=\dfrac{\nu}{\alpha}=\dfrac{\text{Viscous Diffusion}}{\text{Heat Diffusion}}$

Eckert Number (Ec) $=\dfrac{U^2}{c_p\,\Delta T}=\dfrac{\text{Mechanical Energy}}{\text{Thermal Enery}}$

where β is the coefficient of thermal expansion, g is the gravitation vector, ΔT is temperature difference defined as $T_H - T_{inlet}$, U is the reference velocity scale defined as the mean inlet velocity, and ν is the kinematic viscosity of the fluid.

For subsonic flow (i.e. low Mach number) with a moderate Reynolds number, the Eckert number is much smaller than one. Hence the viscous heating term and the flow work term can be neglected. The dimensionless thermal energy equation has the following form:

$$\frac{\partial}{\partial t}\iiint_{\nu}T\,dV+\iiint_{\nu}(\vec{\nabla}\bullet\vec{\nabla})\,T dV=\iint_{\mathcal{A}}\vec{\nabla}T\bullet\vec{n}\,dA$$

A detail derivation of the low Mach number model equations with the Boussinesq approximation is shown by Yam [7].

3) Problem of interest

An experiment with combined forced and free convection in a curved duct has been performed by Cheng and Yeng [8], [9]. In the experiment, a curved duct with a straight long entrance length is fabricated. The straight long entrance length is to ensure a fully developed parabolic velocity profile at the entrance of the heated curved section. (We will later see that this is not always true). A hot water jacker is inserted into the curved section to create the heated section. The heated curved section is then oriented in a vertical upward direction. Room air from a compressor is used as a working fluid inside the assembly. Smoke generated by burning paper straws is injected at the straight duct entrance. Photographs of the secondary flow patterns are taken at the exit of the curved duct where the heated air is discharged directly into the surrounding as jet. A schematic of the experimental apparatus is shown in Figure 1. The parameters used in this experiment (Reynolds number of 59.92 and 246.69, Rayleigh number of 2.57×10^4, curvature ratio of 1:10.9 and Prandtl number of 0.7) are imported in the current numerical study.

4) Numerical Methods

I) Coordinate System

The problems of interest have geometries that are very difficult to describe using a Cartesian coordinate system. Thus, a coordinate transformation is used to define a body fitted coordinate system. For the problems of internal flow in a curved duct with straight duct attached, a three dimensional boundary fitted, non-orthogonal coordinate is used. Typical grid systems for the surface and sections of the curved duct are shown in Figure 2 through 5.

All derivative terms in the equation of motion are evaluated with the use of the generalized coordinates and this involves a coordinate transformation. A detail derivation of the transformation is shown by Dwyer and Dandy [9] and Yam [7].

II) Calculations Of Geometry

The control volume equations (integral equations) consist of volume terms and surface terms. The volume and surface area of a control volume can be obtained by the usage of vector operations. For control volumes with cell centers located at a singular point (like those at the axis of the ellipsoid grid), all the dependent variables can become coupled with the adjacent cell through the convection and viscous terms. This leads to difficulty with implicit solvers. A simple solution to this problem is to put the cell surface at the singular point. As shown by the governing equations, the only terms that exist at the control surface are those of the flux and pressure terms. Since they are being multiplied by the surface area of zero, the excessive coupling is removed. The cell center of the control cell however is still coupled to the rest of the system by the remaining five surfaces. A detail discussion of is shown by Yam [7].

III) Finite Volume Equations

In this study, all the variables are defined at the center of the control cell. When variables are needed at the surface of the cell, averaging is performed, and gradients are evaluated with a second order finite difference with respect to the cell surface. Thus, discretization of the governing equations in generalized coordinates is second order accurate in space. However, for the internal flow, the resulting maximum Reynolds number that we can run to obtain solutions is limited to 200. One way of increasing the Reynolds number is by adding more grid points to the physical domain. This, however, is limited by the capacities of current computers. An alternative is to add artificial dissipation only to the stream wise direction to enhance the stability of the numerical scheme.

This is done by adding $\frac{1}{2}\frac{\vec{V}_\zeta \bullet \vec{ds}_\zeta}{\nu}$ to the diffusion coefficient of the stream wise viscous term where $\vec{V}_\zeta$ is the local stream-wise velocity vector, and $\vec{ds}_\zeta$ is the local length scale of the control volume in the stream-wise direction:

As shown by Yam [7], the areas on the control cell are defined by the cross product of the two position vectors located on each surface. These two position vectors are determined by linear interpolation between the grid points where the surface is located. For a control volume with plane surfaces this is a good method of determining the surface area, however the resulting surface integral of area is not always equal to zero. This can lead to truncation error in the governing equations where surface integrals are evaluated. A typical and an important example is the pressure force term in the momentum equation. The difficulty can be overcome by correcting the pressure force term as:

$$-\iint_A P\,\vec{n}\,dA \Rightarrow -\iint_A P\,\vec{n}\,dA + P\iint_A \vec{n}\,dA$$

Thus any error in the evaluation of the areas is compensated by the second term and the finite volume equations will accept uniform solutions.

IV) Numerical Scheme

After the governing equations have been transformed into finite-difference equations, a numerical scheme must be employed to solve the system of equations. An iterative implicit scheme with replacement (Predictor - Corrector - Corrector) is used in this study. This is variation of the alternate line implicit method with replacement. A detail discussion is shown by Yam [7]. The advantage of using this type of iteration scheme is that it has a fast convergence rate compared to other iterative methods [7].

V) Pressure Solver

The governing equations consist of the continuity equation, three momentum equations, and energy equation with unknowns of U, V, W, P and T. The velocity field is obtained through the momentum equations, and the temperature field is obtained from the thermal energy equation. However, we do not have an explicit equation for the pressure field. Thus, special treatment must be used in order to obtain the pressure field. The method that was used to obtain pressure for this study is a variation of the method developed by Chorin [8]. A detail discussion is shown by Yam [7].

VI) Initial Conditions And Boundary Conditions

Due to the elliptic nature of the governing equations, boundary conditions must be given at all boundaries. Moreover, since all variables are a function of both space and time, initial conditions for all variables must also be given. For mass driven internal flow, the mass flow rate is the only known quantity. The pressure gradient (pressure drop) is a result from the balancing of the forces on the fluid particles. Thus, velocity and pressure are unknowns everywhere. For the combined forced and free convection flow, it is assumed that the duct has a long straight inlet section such that before the entry of the heated curved section, the flow is fully developed. Thus the velocity field is assumed to be parabolic everywhere. The pressure field is assumed to have a uniform pressure gradient along the duct system. For the temperature field, it is assumed that the temperature is uniformed everywhere and is equal to the inlet temperature.

The boundary conditions for the velocity and the pressure fields are more complicated. At the surface of the duct, the no-slip velocity still holds. A zero pressure gradient is applied at the surface. The velocity profile at the inlet is also fixed and is that of the parabolic profile. Hence the velocity correction is specified to be zero. The pressure, however, is to be extrapolated from the pressure at first cell next to the inlet. This will allow the inlet pressure to change in order to satisfy the balance of momentum at the first control cell. At the exit, the velocity field is assumed to be fully developed. Thus, the velocity gradient along a stream line is zero. Again, we extrapolate the pressure for the exit pressure field. For the temperature boundary conditions, the wall temperature at the straight section is equal to zero while the temperature at the curved section is equal to one, The inlet temperature is held constant with a value of zero. At the exit, the temperature field is assumed to be fully developed. Thus, the temperature gradient along a stream line is set to be zero.

As a comparison, a pure forced convection through a 180 degree bend duct with straight ducts attached is included in this study. However, the inlet straight section of this case is relative short. It is reasonable to assume that the flow at the inlet is mainly composed of an inviscid core since the boundary layer has not yet been established. Thus the initial condition for the velocity field is assumed to be an inviscid velocity profile with zero velocity at the wall everywhere. For the temperature, the initial and boundary conditions are the same as the above case with the exception that the straight section is also heated.

A summary of initial and boundary conditions for this case is listed in Table 1.

Table 1
Initial and Boundary Conditions for Forced and Free Convection (Mass Driven) Internal Flow

	Velocity	Temperature	Pressure
Initial Conditions	$\vec{V} = \vec{V}(\xi,\eta)$	$T = 0$	$P = P(\xi,\eta)$
Body Boundary Conditions	$\vec{V} = 0$	$T = T_{wall}$	$\frac{\partial P}{\partial \eta} = 0$
Far Field Upstream Boundary Conditions	$\vec{V} = \vec{V}(\xi,\eta)$	$T = 0$	P=Calculated from the flow field.

Far Field Down-stream Boundary Conditions	$\frac{\partial \vec{V}}{\partial \vec{s}} = 0$	$\frac{\partial T}{\partial \vec{s}} = 0$	P=Calculated from the flow field.

5) Discussion Of Results

A primary objective of this study is to determine the surface (normal and shear) stresses, surface heat flux and the internal flow structure inside a straight-curved duct subject to a combined forced and free convection. With the gravity vector parallel to the plane of symmetry of the geometry of this problem, and with the assumption that the flow is symmetric in the cross-section of the duct, only half of the domain needs to be computed. (Hence symmetrical boundary conditions of all gradients equal to zero and the velocity vector tangent to the plane of symmetry are imposed at the plane of symmetry.)

We have placed 15 geometrically stretched (of 11 percent) grid points in the radial (η) direction, 19 geometrically stretched (of 9 percent) grid points in the circumferential (ξ) direction and either 46 or 61 grid points in the stream-wise (ζ) direction. By stretching in the radial direction, we have a grid system that can capture the boundary layer next to the wall. The stretching in the circumferential direction allows us to obtain a more accurate secondary flow in a curved duct. A typical example of the grid system used in the curved duct problem is shown in Figures 2 to 5. A dimensionless time step (Δt) of 0.1 is used in these calculations. A Prandtl number of 0.7 is used through out this study.

A) Accuracy

The formulation of the internal flow part of the code is tested by running a series of steady state test cases. Steady state is assumed to be reached when the divergence of the velocity field is dropped to machine zero and the relative change in the velocity field is in the order of 10^{-4}. This generally takes 1200 time steps. The resulting velocity profile of the test case is compared with the exact solution. For the mass driven case with an inviscid inlet velocity being prescribed, the entrance length before the flow becomes fully developed in a straight duct is calculated and is compared with experimental correlations. The resulting pressure drop, and velocity profiles at the fully developed region are compared with the exact solutions. The comparison is good since the errors in velocity and in pressure drop are in the order of discretization error.

Two test cases of mass driven flow in a 180 degrees curved duct, curvature ratio (ratio of curved duct radius R_{duct} to the main curved radius R_{curve}) of $\frac{1}{7}$ with Reynolds number of 242 and 900 are calculated. The resulting speed contour and secondary flow field are then compared with the numerical results obtained by Soh and Berger [4] with excellent agreement. A detail discussion of the solutions and comparison is shown by Yam [7].

For internal flow the mean temperature is defined as

$$T_{mean} = \frac{\iint T\vec{V}\bullet\vec{n}\,dA}{\iint \vec{V}\bullet\vec{n}\,dA}$$

while the local Nusselt Number is defined as

$$Nu = \frac{h R_o}{k} = -\frac{\frac{\partial T}{\partial r}}{T_{mean} - T_{wall}}$$

and can be viewed as the ratio of the heat flux due to convection and the heat flux due to conduction. A high Nusselt number means heat transfer is dominated by convection while a low Nusselt number means heat transfer is done mainly by conduction.

To test the evaluation of the local heat transfer rate, a test case of fluid with inlet temperature of 1 and cooled wall temperature of 0 in a straight duct is calculated. The mean temperature and the Nusselt number are calculated and the results are then compared with theoretical values with excellent agreement.

B) Detail Results

Case I : Re = 59.92, Ra = 2.57×10^4, Pr = 0.7

We begin the study with a curvature ratio of $\frac{1}{10.9}$, Reynolds number of 59.92, Rayleigh number of 2.57×10^4 and Prandtl number of 0.7. A total of 19×15×61 grid points are used in this study.

At this Reynolds number, the entire flow field is dominated by buoyancy affects. The resulting pressure contour at the plane of symmetry and the pressure contour at the surface of the duct are shown in Figures 6 and 7. It is clear that the pressure distribution has taken the form of hydrostatic.

The pressure at the inner wall, at the center line of the duct and at the outer wall verses the K-station (where K equals 1 is at the inlet, while K equals 61 is at the exit) as shown in Figure 8. The reason for plotting the pressure against the K-station is that there is no obvious physical length scale one can plot the pressure. The number of the K-station can be viewed as the transformed length scale ζ. Thus, this is one way of presenting combined results in straight and curved sections in a one-dimensional plot. The unusual reverse of the maximum and minimum value location at the cross-section of the duct is a characteristic of hydrostatic pressure distribution inside a curved duct.

The cross flow velocity field is shown by the velocity vector plot at the symmetry (X-Z) plane (Figure 9). At the inlet, the velocity profile is parabolic as discussed previously. As the fluid particles enter the curved section, heat is added to it. With the combined influence of the buoyancy and inertia

forces, the fluid particles tend to move to the highest portion of each cross section the duct. This is shown by the maximum velocity located at the inner bend of the duct as indicated in Figure 9. In order to satisfy mass balance at each section, those fluid particles at the outer bend where buoyancy force is relative weak (when compare to those at the inner bend) have to flow backwards. This reversed flow at the outer wall travels upstream of the curved section to the straight section due to the low inertia of the fluid particles as indicated in Figure 9. The flow field has this nature until 80 degrees of the bend, when both inertia force and buoyancy force acted in phase to push the fluid particles upwards. The speed contour (Figure 10) at the plane of symmetry clearly shows the reversed flow region at the outer bend of the curved inlet.

As the flow continue to develop, the centrifugal and buoyancy forces act together and continue pushing the fluid particles downstream where a reversed flow at the inner bend is then observed. As the flow continues to develop, the maximum velocity location starts moving towards the outer bend. As the flow reaches the exit, the buoyancy and centrifugal forces act out of phase and the maximum velocity is located near the outer bend. The corresponding surface total shear stress is shown in Figure 11. It is clearly shown that the maximum surface shear stress is located at the inner bend of the curved entrance region due to the high velocity gradient at that location. The minimum shear stress region (with an opposite sign due to the reversed flow) is located at the inner bend immediately downstream of the maximum region. The speed contour at the 80 degree cross section where the reversed flow region exists at the outer bend is shown in Figure 12. A secondary flow is also observed at the exit of the duct as indicated by the velocity vector plot at the exit plane as shown in Figure 13. The center of the secondary flow is located at the top half of the duct due to the strong buoyancy force.

From the temperature contour at the symmetry plane (Figure 14), we can see that thermal boundary layer formed rapidly at the inner bend of the curved section and is confined to a thin layer. At the outer wall, the thermal boundary layer flows backwards to the straight section before convecting downstream. This is due to the reversed flow (shown by the velocity vector plot at the symmetry plane in Figure9), where fluid particles that have been heated up by hot curved wall have convected backwards to the straight inlet section.

The temperature contour at the exit plane is also shown in Figure 15. We can see that the temperature gradient at the outer wall is at a maximum while the temperature gradient at the inner is at a minimum. Since temperature can be view as a passive scalar, the temperature contour can provided us a view of the flow field. Comparison of the temperature contour at the exit (Figure 15) with the secondary flow smoke pattern (Figure 16) obtained by Cheng and Yuen [8] where the Reynolds number, Rayleigh number and curvature ratio is identical to this case is then made.

From Figure 16, we can see that the buoyancy force is pushing all the smoke towards the outer bend and is confined to the top 30 percent of the cross-sectional area. Since at this Reynolds number, the centrifugal force is relative weak, the flow field is dominated by the buoyancy force. Moreover the secondary flow is not strong enough to push the smoke from the outer wall back towards the inner wall. This is qualitatively comparable to the temperature contour (Figure 15) where the temperature contour lines done not indicated a downward flow motion next to the wall. (The detection of downward motion is detacted by the curvature of the contour lines and will become clear when a higher Reynolds number case is discussed in a later section)

The local Nusselt number at the inner bend, at the top of the duct, and at the outer bend are calculated and are shown in Figure 17. From this local Nusselt number plot, the heat transfer rate at the inner bend of the curved inlet section has increased from a Nusselt number of 6.9 to 8.6 (where the shear stress is at a maximum) then decreased back to 0.7. This is caused by the thermal boundary layer being pressed into the inner wall by the buoyancy force. As this boundary layer lifts off from the inner wall, the resulting heat transfer rate drops to zero. At the outer wall, the reverse of this affect is observed. The Nusselt number remains closed to zero at the beginning of the curved section where reversed flow is observed. At about 80 degrees into the bend, the Nusselt number started to increase up to 6.8 (at 120 degrees) and remains constant. At the center of the duct, the nusselt number takes on a more convectional form of having a maximum value of 7.0 at the entrance of the heated section and the continues to drop to a constant value of 1.9. This shows that the heat transfer rate in a straight-curved duct is higher than that of a straight duct where the Nusselt number for a fully developed flow base on radius has a value of 1.8.

The mean duct temperature is shown in Figure 18. The mean temperature increases from 0 at the beginning of the duct (at the straight section) and drops back down to zero at the beginning of the heated section. This is due to the reversed flow of the heated fluid flow at the inlet section. As the flow continues to develop, the mean temperature continues to increase to 0.98 at the duct exit.

Case II : Re = 246.69, Ra = 2.57×10^4, Pr = 0.7

The second case presented here is for a Reynolds number of 246.69, Rayleigh number of 2.57×10^4 and Prandtl number of 0.7. The curvature ratio and grid density are the same as Case I.

At this Reynolds number, the buoyancy affect dominates the region next to the inner wall at the last half or the duct while the centrifugal force influences the region next to the outer wall of the entire duct system. This is shown by the pressure contour at the plane of symmetry in Figure 19. We can see that the pressure contour has taken the form of hydrostatic (parallel line with respect to the horizon) at the inner wall while centrifugal force (contour lines curved upward) is evident at the outer wall. The pressure at the inner wall, at the center line of the duct and at the outer wall are also presented as the function along the duct in Figure 20. The unusual reverse of the maximum and minimum value which is a characteristic of hydrostatic pressure distribution inside a curved duct occurs near the exit of the duct while the

centrifugal force dominated pressure distribution is observed at the first half of the curved section.

The cross flow field is shown by the velocity vector plot at the symmetry (X-Z) plane (Figure 21). As the fluid particles enter the curved section, heat is added to it. With the combined influence of the buoyancy and inertia forces, the fluid particles tend to move to the highest portion of each cross section the duct. This is shown by the maximum velocity located at the inner bend of the duct as indicated in Figure 21. In order to satisfy mass balance at each section, those fluid particles at the outer bend where buoyancy force is relative weak (when compare to those at the inner bend) have to flow backwards. However, unlike Case I, the incoming fluid has enough inertia such that reversed flow does not occur at the straight inlet section. The reversed flow at the outer wall continues up to 60 degrees of the bend. At the 55 degree location, both inertia and buoyancy force have accelerated the fluid particles in phase such that a reversed flow at inner bends is observed. (Hence a reversed flow at both the outer and inner bends is detected from 55 to 60 degrees). Moreover, the maximum velocity location has shifted from the region next to the inner bend to the region next to the outer bend. The combined forced and free convection is so strong that the reversed flow at the inner bend continues up to 150 degrees of the curved section. As the flow continues to develop, the maximum velocity location moves towards the outer bend. As the flow reaches the exit, the buoyancy and centrifugal forces act out of phase and the maximum velocity is located near the outer bend due to the centrifugal force. Speed contours at the plane of symmetry are also shown in Figure 22. The reversed flow at the beginning of the outer bend and at the mid-section of the curved duct is clearly shown. The corresponded surface total shear stress is shown in Figure 23. The maximum surface shear stress is located at the outer bend of the curved section due to the high velocity gradient. The minimum shear stress regions (with an opposite sign due to the reversed flow) are located at the outer bend at the beginning of the curved section and at the inner bend of the last half section.

A secondary flow is observed at the 75 degrees station and is shown in Figure 24. The speed contour at the location where the reversed flow at the inner bend is shown in Figure 25. A secondary flow is observed at the exit of the duct as indicated by the velocity vector plot at the exit plane as shown in Figure 26. We can see that the center of the secondary flow is located at the mid section and the strength of the secondary flow is stronger than that of case one due to the strong centrifugal effect. The speed contour at the exit where the high velocity gradient is located next to the outer bend is shown in Figure 27.

From the temperature contour at the symmetry plane (Figure 28), we can see that thermal boundary layer formed rapidly at the inner bend and is confined to a thin layer while the thermal boundary layer at the outer bend grows rapidly due to the buoyancy force. As the duct turned, the combined buoyancy and centrifugal forces have lifted the thermal boundary layer away from the inner bend and pushed it against the outer bend where the thermal boundary layer formed tightly against the outer wall. The temperature contour at the exit plane is also shown in Figure 29. We can see that the temperature gradient at the outer wall is at maximum while the temperature gradient at the inner is at minimum. Furthermore, the maximum temperature region is closer to the outer bend when compare to the lower Reynolds number case (Figure 15) due to the higher centrifugal force.

From the secondary flow pattern (Figure 30) obtained by Cheng and Yuen [8] with the same Reynolds number, Rayleigh number, Prandtl number and curvature ratio, we can see that the smoke at the outer bend has been convected towards the inner bend by the stronger secondary flow. The smoke has occupied 70 percent of the cross-sectional area. This is qualitative comparable to the temperature contour (Figure 29) where the temperature contour lines shows a concave down shape which indicated that it is being bend by the downward flow at the duct wall region.

From the local Nusselt number plot (Figure 31), the heat transfer rate at the inner bend of the curved inlet section has a Nusselt number of 8.6 and then continue drop to a low value of 0.183 where the thermal boundary layer have lift off the inner bend (K=31). The Nusselt number there increases slightly and has a value of 0.45 as the flow exits the duct. At the outer wall, the Nusselt number has a maximum of 3.12 at the beginning of the heated section and then drops back to have a low value of 0.2. This is the location where the thermal boundary layer has lifted off from the outer wall due to the buoyancy effect. At K=25, the Nusselt number started to increase rapidly to a high value of 13.5. This is due to the reattachment of the thermal boundary layer being pushed to the outer wall by the combined effect of buoyancy and centrifugal forces.

The mean temperature along the duct is shown in Figure 32. The mean temperature has increased from 0 to 0.82 at the duct exit. This shows that even though the Nusselt number reached an asymptotic value, the flow is not thermally fully developed.

Case III : Re = 242, Ra = 0, Pr = 0.7

For comparison, a similar forced convection case without body force is present here. A curvature ratio of $\frac{1}{7}$, Reynolds number of 242, Prandtl number of 0.7 is used in this case. A total of 21×15×46 grid points are used in this study. The grids in the straight duct section and in the stream-wise direction are expanded geometrically by 10 percent. The resulting grid system is shown in Figures 3, 4 and 5. The flow is driven by an imposed mass flow rate thus the only known quantity is the velocity field at the inlet. The initial and boundary conditions used for this case have already been discussed in the initial and boundary conditions section.

The calculated pressure distribution is presented by plotting, (1) the pressure at the inner bend, (2) the pressure at the center line of the duct, and (3) the pressure at the outer bend verses the K-station as shown in Figure 33. The resulting pressure contour at the plane of symmetry and the pressure contour at the surface of the duct are also shown in Figures 34 and 35. From the pressure profile, Figure 33, the inlet pressure at the center is slightly lower than the pressure at the wall. This is caused by the inlet flow still being mainly composed of an

inviscid core with a boundary layer starting to develop. As the boundary layer grows, the displacement thickness also grows. This increase of the displacement accelerates the main inviscid core in order to maintain the mass balance. By Bernoulli's law, as the velocity increases, the pressure decreases. Thus the pressure is lower at the center. As the fluid enters the curved section, the pressure at the outer bend is higher than the pressure at the inner bend. This is due to the centrifugal force exerted at the duct wall by the fluid particles. Note that at the outer wall of the entrance region of the curved section, the pressure gradient is almost zero. Although there is a slight pressure oscillation at the exit of the curved section, this is due to the lack of resolution of grid points in the stream-wise direction. This problem can be over come by adding more grids to the stream-wise direction.

From the surface pressure contours, Figure 34, there is a pressure drop along the straight section of the duct, however, the pressure is almost uniform across the duct. We can also see that from Figure 34, not only is there a pressure difference between the inlet and the exit, but also a pressure difference between the inner bend and the outer bend due to the centrifugal force acting by the fluid. At the outer bend of the entrance of the curved section there is a region where the pressure is uniform and it is shown in both pressure contours at the plane of symmetry, Figure 34, and at the surface of the bend duct, Figure 35. This is due to the increase of the pressure by the centrifugal force acting at the curved section. Unlike the combined forced and free convection, here the pressure at the outer bend remains higher then the pressure at the inner bend of the same cross section throughout the curved section.

The velocity profile for this case is significantly different than that of case II. Unlike case II where the maximum velocity location started off at the inner bend and later on moved to the outer bend, the maximum velocity location started off at the region next to the outer bend and remained at the outer bend. A detail description of the flow development is discussed as follows.

The velocity profile (Figure 36) at the inlet is an inviscid one which is explicitly specified. As the flow enters the straight inlet section, the boundary layer started to grow, however due to the shortness of the straight section, the flow is still composed mainly of an inviscid core. As the fluid particles enter the curved section, the velocity profile tends to build up at the outer wall. This is due to the particles coming from the straight section still want to go straight by their momentum. However, because of the existence of the solid curved wall, the fluid particles have no choice but to change their course to follow the curvature of the duct. This lead to a larger buildup of the fluid particles at the outer wall. The existence of an inviscid core (where velocity shows a flat plateau) can still be observed up to the 45 degrees station of the curved section. The developing region exists to about 110 degrees until the flow in the curved section becomes fully developed. (Further study by Yam [7] has indicated the existent of the inviscid does not have major influence in the heat transfer part of the problem). At the fully developed region, the velocity profile has the maximum located closed to the outer wall. The speed contour at 90 degrees section of the curved duct is shown in Figure 37. A secondary flow is also observed and is shown by the secondary flow velocity vector located at the 90 degrees section in Figure 38. As the fluid exits the curved section and enters the straight section, the maximum velocity is still located toward the outer wall. The speed contours at the exit plane is shown in Figure 39. The cross velocity vector at the exit is also shown in Figure 40. The secondary motion is still clearly defined with the center of the secondary flow located at the lower region of the cross section. Without the influence of the buoyancy force, the secondary flow is strong enough to move some of the fluid particles towards the inner bend as indicated by the concave downward shape of the speed contour line. (Without body force, the temperature contours are the same as the speed contours).

The total surface shear stress contour is shown in Figure 41. There is a large area of minimum shear stress located at the inner bend with a large area of maximum shear stress located at the outer bend. This is obvious from the velocity vector plot (Figure 36), we can see that the velocity gradient is higher at the outer bend then at the inner bend. At about 80 degrees from the inner bend, a small region of maximum change in the shear stress is observed in Figure 41. From the secondary flow velocity vector plots (Figure 40), we can see that the center of the secondary flow and the maximum secondary velocity gradient are located at about 80 degrees from the inner bend. This indicates that the region of maximum changes in shear stress at the surface of a curved duct has the same angle that is between the center of the secondary flow and the plane of symmetry.

From the temperature contour at the symmetry plane (Figure 42), we can see that a thermal boundary layer formed rapidly at the outer bend and is confined to a thin layer. At the inner wall, the thermal boundary layer formed at the straight section continues to grow at the curved section and eventually disappears. Unlike the combined forced and free convection case, the thermal boundary layer at the outer bend never lifts off the duct wall. The thermal boundary layer (Figure 42) at the inner wall start growing rapidly as it enters the curved section while for the combined forced and free convection case (Figure 28), the separation of the thermal boundary layer has delay up to 55 degrees into the curved section.

The mean temperature and the local Nusselt number at the inner bend, at the top of the duct, and at the outer bend are shown in Figures 43 and 44. Unlike the combined forced and free convection cases where the Nusselt number at the inner bend first has a high value and then at outer bend has a high value (Figure 17, Figure 31), the forced convection case has a higher Nusselt number at the outer bend than when compared to the inner bend at all location (Figure 43). From the local Nusselt number plot (Figure 43), the heat transfer rate at the inlet section is decreasing uniformly across the duct. As the flow enters the curved section, the heat transfer rate at the outer bend continues to increase from a Nusselt number of 2.7 to 9.8 towards the end of the curved section while the Nusselt number at the inner bend continues to decrease to a steady value of 0.6. This shows that the heat transfer rate at the outer bend is 5.4 times higher than that of a straight duct (Nusselt number of 1.8). At the inner bend, however, the heat transfer rate is about 3 times lower than that of a straight duct. The heat transfer is about 16 times higher at the outer bend when

compared to the heat transfer at the inner bend. This is reasonable because the fluid particles are convected into the wall at a much higher rate at the outer bend then that at the inner bend. The overall heat transfer rate in a curved duct is also higher than that of a straight duct. This is due to the secondary fluid motion that enhances the heat transfer. As the fluid leaves the curved section to enter the straight section, the Nusselt number at inner bend and at center start to decrease while the Nusselt number at the inner bend starts to increase. If the straight duct section at the exit is long enough, one can expect that the Nusselt number will approach the value of the straight duct (i.e. Nusselt number of 1.8). The resulting surface heat flux contour (Figure 45) shows that the region at the inner bend has a lower heat flux value than the region at the outer bend.

6) Conclusion

Solutions for the combined free and forced convection in a curved duct are obtained by solving the low Mach number model of the Navier-Stokes equation using a control volume method. The control volume method has the advantage of clear physical interpretation of the equations. From this study we have concluded the following:

(1) The maximum velocity is located near the inner bend at the beginning of the curved section and it transfers towards the outer bend as the flow developed. The region where maximum velocity located near the inner bend is buoyancy force dominated while the region where velocity located near the outer bend is a result of the combined buoyancy and centrifugal forces.

(2) Reversed flow exists at the beginning of the outer bend of the curved duct. This is due to the strong buoyancy force which entrains fluid particles upwards. Fluid with lower momentum have to flow backwards in order to maintain mass balance.

(3) Reversed flow exists at the inner bend of the last half section of the curved duct. This is due to the strong combined inertia, centrifugal and buoyancy forces that accelerate the fluid particles at the outer bend forward. Again this reversed flow is a necessary condition for the conversation of mass.

(4) Secondary flow exists in the flow structure. At lower Reynolds number, the strong buoyancy force has reduced the effectiveness in mixing. This was observed by Cheng and Yuen [8] who photographed smoke patterns confined to the upper area of the duct at low Reynolds number. As the Reynolds number increased, the strength of the secondary flow increased and pushed the smoke towards the inner bend.

(5) A negative Nusselt number is present at the straight section for the lower Reynolds number case. This is due to the backward flow from the heated section. Instead of heat being deposited into the fluid (which yields positive Nusselt number), heat is being deposited back to the duct by the reversed flow of the hot fluid.

(6) Nusselt number at the inner bend is high at the beginning of the heated section. This is due to the buoyancy force that pushed the thermal boundary layer against the inner bend which lead to a high temperature gradient. As the flow developed, the thermal boundary layer will lift off the inner bend and pressed against the outer bend thus lead to a high Nusselt number at the outer bend at the last half of the curved section.

When comparing the combined forced and free convection results with the forced convection results, we notice that:

(1) The maximum velocity location for the forced convection is next to the outer bend due to the centrifugal force in the entire flow field.

(2) There is no reversed flow exist in the entire flow field for the forced convection.

(3) The secondary flow is stronger for the forced convection case when compared to the combined forced and free convection case due to the lack of the buoyancy force.

(4) Heat transfer rate at the outer bend is always stronger than that at the inner bend for the pure forced convection case. This is due to the centrifugal force that pushes the thermal boundary layer closed to the outer wall.

References

1. Dean, W. R. "Note On The Motion Of Fluid In A Curved Duct", Phil. Mag. 20, 208, 1927.

2. Dean, W. R. "The Streamline Motion Of Fluid In A Curved Duct", Phil. Mag. 30, 673, 1928.

3. Masliyah, J. H., "on Laminar Flow In Curved Semicircular Ducts", J. Fluid Mech. (1980), Vol. 99, part 3, pp.469-479.

4. Soh, W. Y. and Berger, S. A., "Laminar entrance flow in a curved duct", J. Fluid Mech. (1984), Vol. 48, pp 109-135.

5. Soh, W. Y. and Berger, S. A., " Fully developed flow in a curved duct of arbitrary curvature ratio", International Journal For Numerical Methods in Fluid, Vol. 7, pp. 733-755, 1987.

6. Yao, L. Y. and Berger, S. A., "Flow in heated curved ducts", J. Fluid Mech. (1978), Vol. 88, pp. 339-354.

7. Yam, C. "An Investigation of Flow Structure and Heat Transfer Characteristics of Three Dimensional Flows", (1991) Ph.D. Dissertation. University of California, Davis.

8. Cheng, K.C. and Yuen, F. P. "Flow Visualization Experiments on Secondary Flow Pattens in an Isothermally Heated Curved Duct", Journal of Heat Transfer .(1987), Vol. 109, pp.55-61.

9. Cheng, K.C. and Yuen, F. P. "Flow Visualization Studies on Secondary Flow Pattens in Straight tubes Downstream of a 180 deg Bend and in Isothermally Heated Horizontal Tubes", Journal of Heat Transfer .(1987), Vol. 109, pp.49-54.

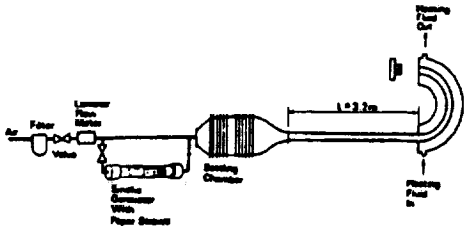

Figure 1
Schematic Diagram of Experimental Apparatus by Cheung and Yuen [8]

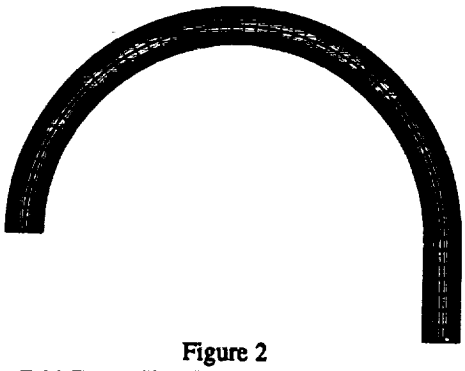

Figure 2
Grid System For The Straight-Bend Duct (X-Z Plane)

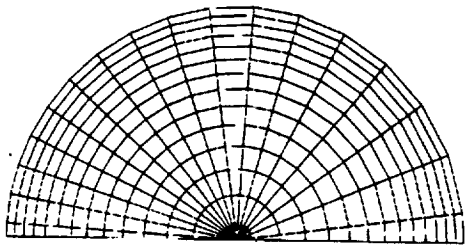

Figure 3
Internal Grid System

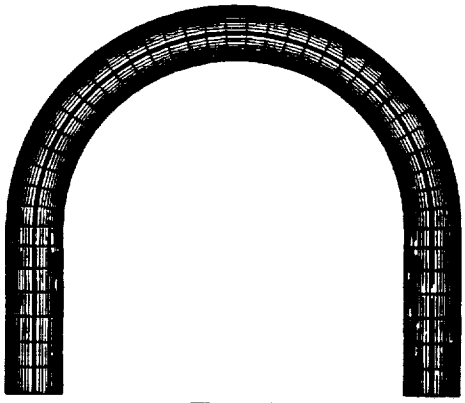

Figure 4
Grid System For The 180 Degrees Bend Duct With Straight Ducts Attached

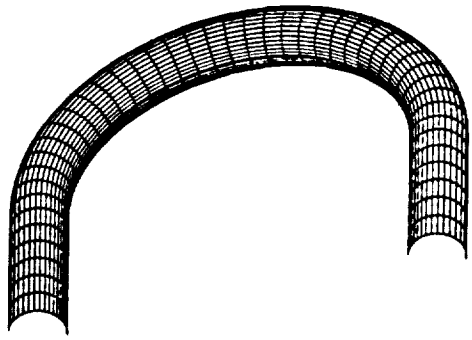

Figure 5
Surface Grid For The 180 Degrees Bend Curved Duct With Straight Ducts Attached

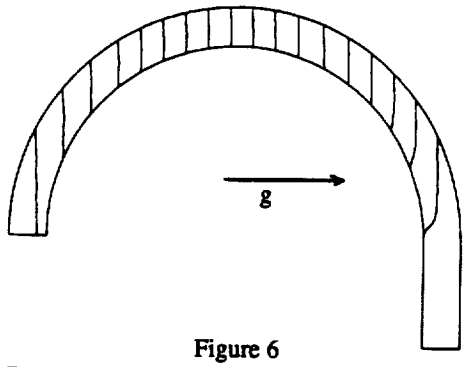

Figure 6
Pressure Contour At The Plane Of Symmetry
Re = 59.92, Ra = 2.57e4

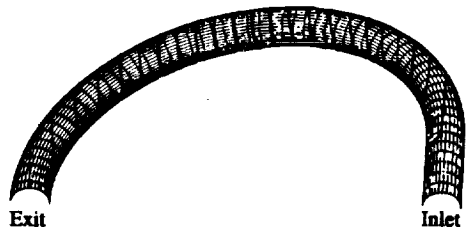

Figure 7
Surface Pressure Contour
Re = 59.92, Ra = 2.57e4

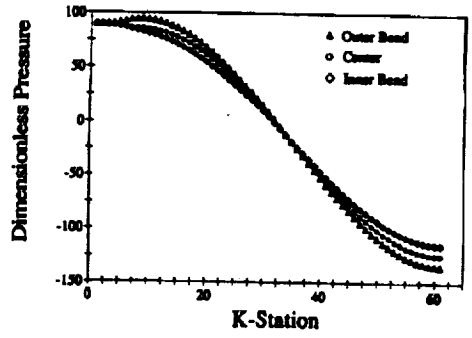

Figure 8
Pressure Along The Duct
Re = 59.92, Ra = 2.57e4

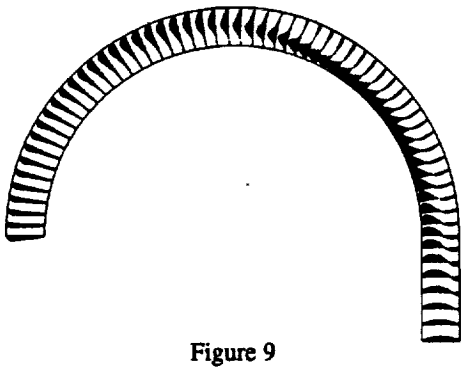

Figure 9
Velocity Vector At The Plane Of Symmetry
Re = 59.92, Ra = 2.57e4

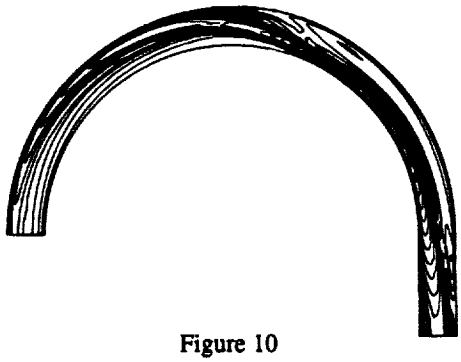

Figure 10
Speed Contour At The Plance Of Symmetry
Re = 59.92, Ra = 2.57e4

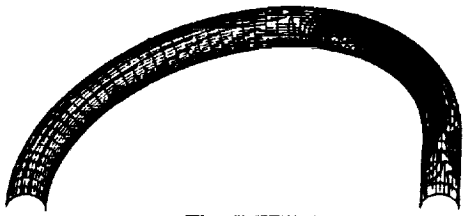

Figure 11
Total Surface Stresses
Re = 59.92, Ra = 2.57e4

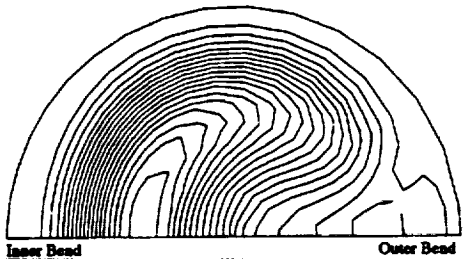

Figure 12
Speed Contour At The 80 Degrees Location
Re = 59.92, Ra = 2.57e4

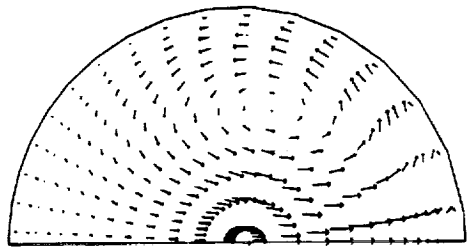

Figure 13
Secondary Flow At The Exit
Re = 59.92, Ra = 2.57e4

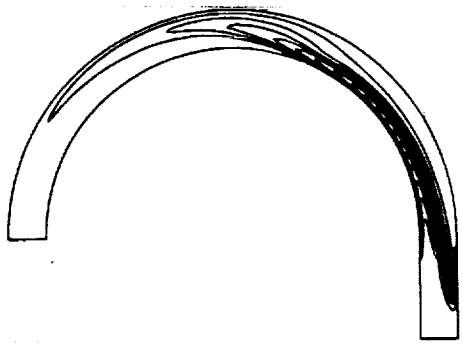

Figure 14
Temperature Contour At The Plane Of Symmetry

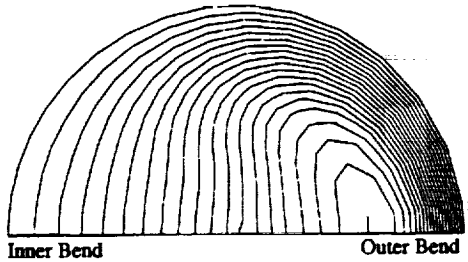

Figure 15
Temperature At The Exit

Figure 16
Smoke Pattern At The Exit Obtained By Cheng And Yuen [8]

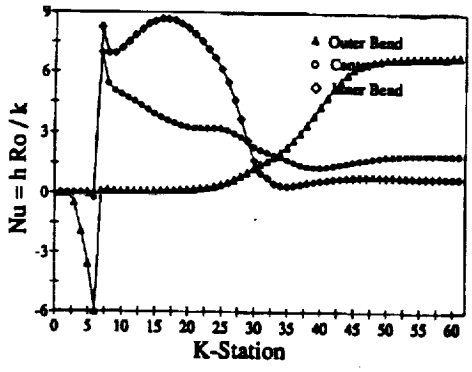

Figure 17
Nusselt Number Along The Duct
Re = 59.95 Ra = 2.57e4

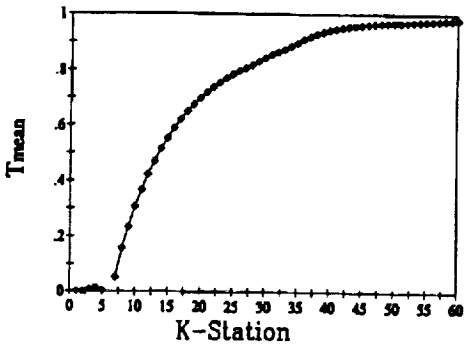

Figure 18
Mean Temperature Along The Duct
Re = 59.92, Ra = 2.57e4

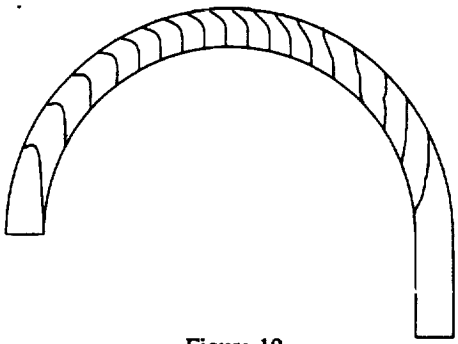

Figure 19
Pressure At The Plane Of Symmetry
Re = 246.69, Ra = 2.57e4

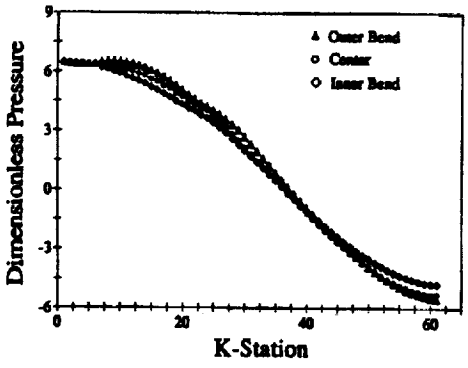

Figure 20
Pressure Along The Duct
Re = 246.69, Ra = 2.57e4

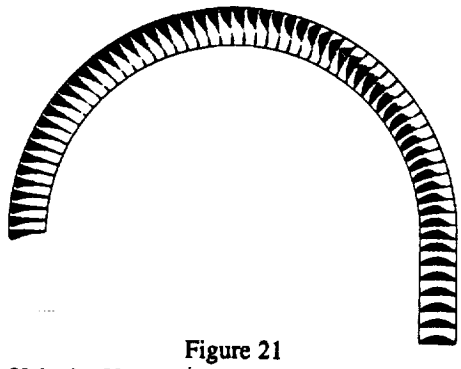

Figure 21
Velocity Vector At The Plane Of Symmetry
Re = 246.69, Ra = 2.57e4

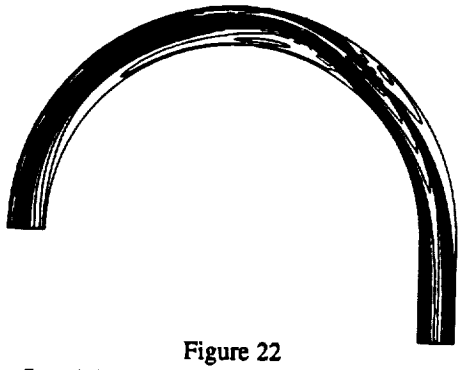

Figure 22
Speed Contour At the Plane of Symmetry
Re = 246.69, Ra = 2.57e4

Figure 23
Total Surface Stresses
Re = 246.69, Ra = 2.57e4

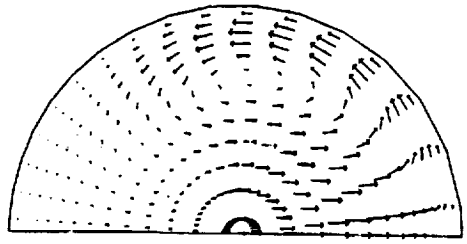

Figure 24
Secondary Flow At The 75 Degrees Location

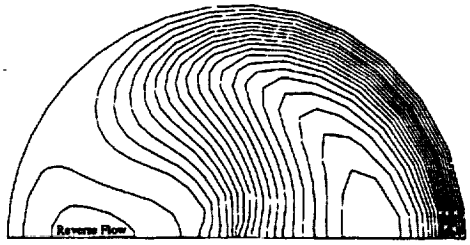

Figure 25
Speed Contour At the 75 Degrees Location

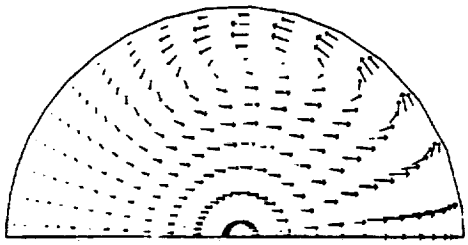

Figure 26
Secondary Flow At The Exit

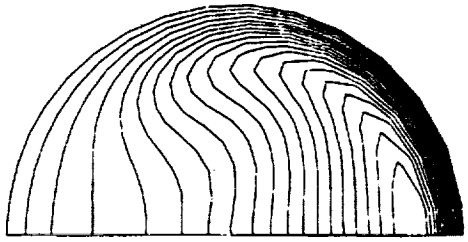

Figure 27
Speed Contour At The Exit

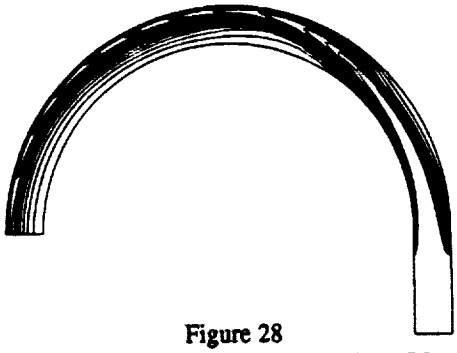

Figure 28
Temperature Contour At The Plane Of Symmetry

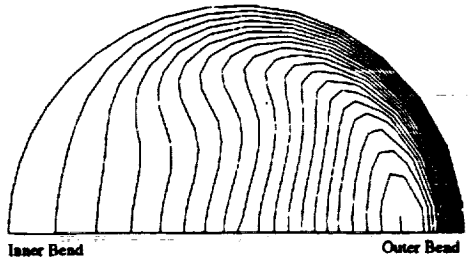

Figure 29
Temperature Contour At The Exit

Figure 30
Smoke Pattent At The Exit Obtained By Cheng And Yuen [8]

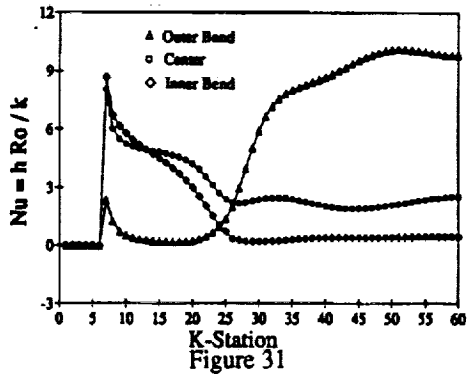

Figure 31
Local Nusselt Number Along The Duct
Re = 246.69, Ra = 2.57e4

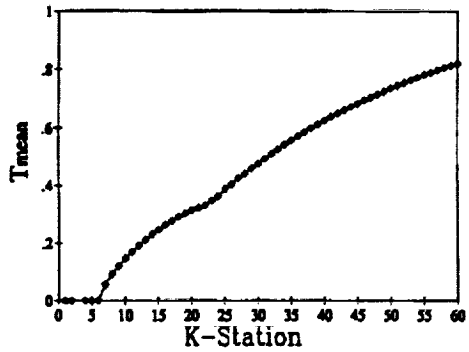

Figure 32
Mean Temperature Along The Duct
Re = 246.69, Ra = 2.57e4

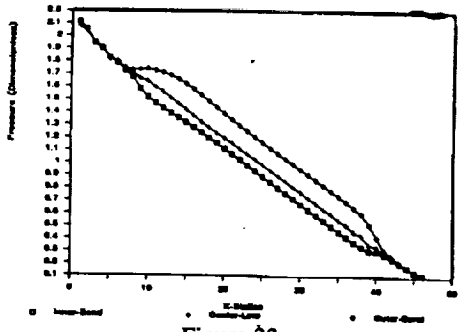

Figure 33
Pressure Along The Duct
Re = 242, Ra =0.0

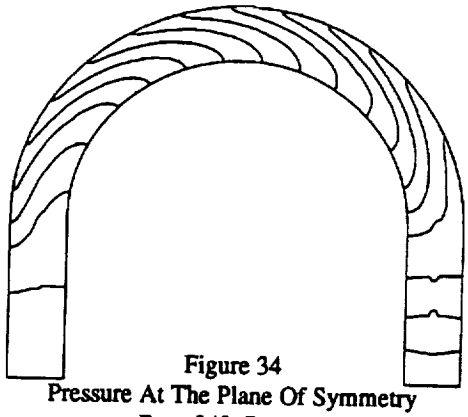

Figure 34
Pressure At The Plane Of Symmetry
Re = 242, Ra =0.0

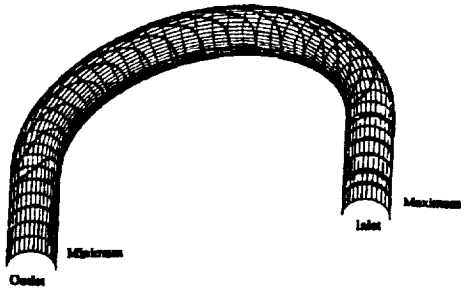

Figure 35
Surface Pressure Contour
Re = 242, Ra =0.0

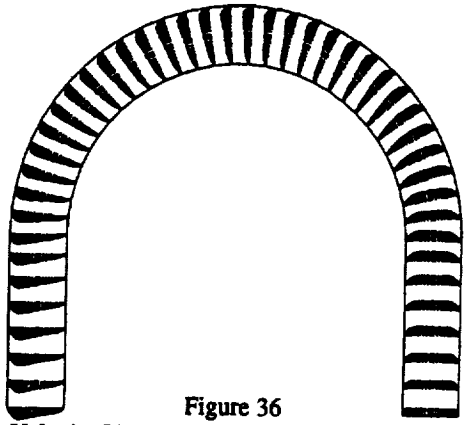

Figure 36
Velocity Vector At The Plane Of Symmetry
Re = 242, Ra =0.0

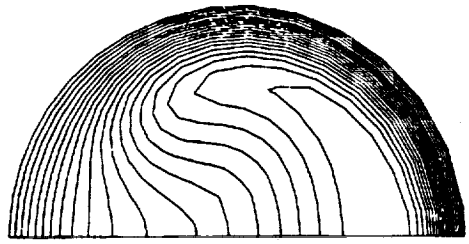

Figure 37
Speed Contour At the 90 Degrees Location

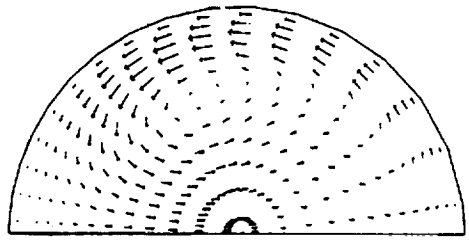

Figure 38
Secondary Flow At The 90 Degrees Location

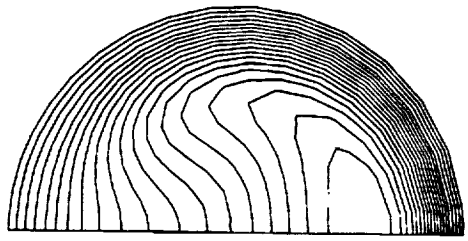

Figure 39
Speed Contour At The Exit

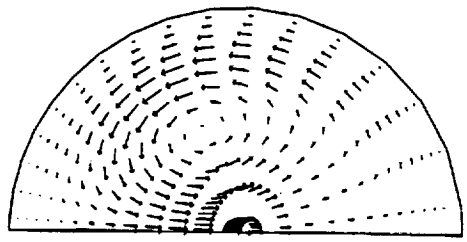

Figure 40
Secondary Flow At the Exit

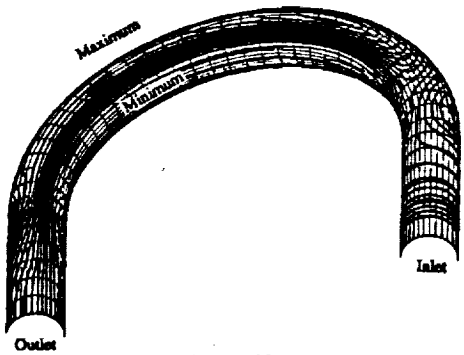

Figure 41
Total Surface Stresses
Re = 242, Ra = 0.0

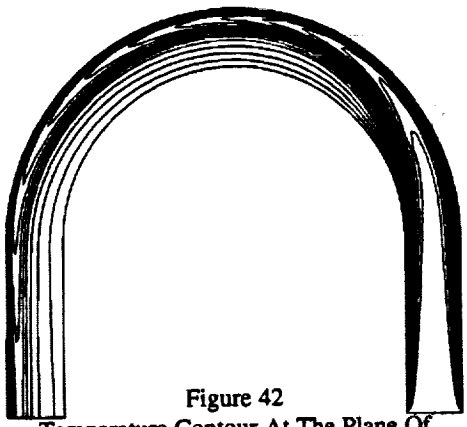

Figure 42
Temperature Contour At The Plane Of Symmetry

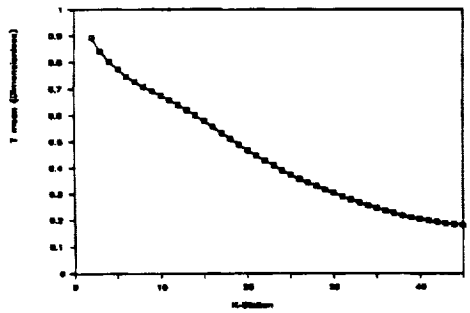

Figure 43
Mean Temperature Along The Duct

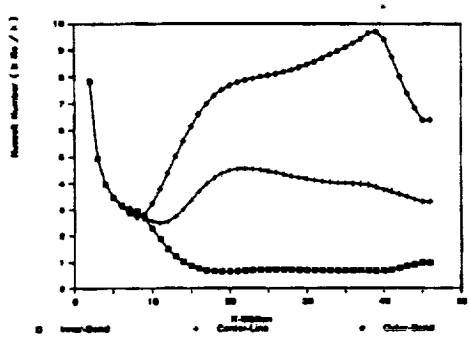

Figure 44
Local Nusselt Number Along The Duct

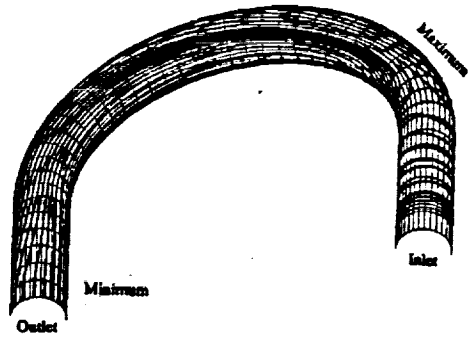

Figure 45
Surface Heat Flux
Re = 242, Ra =0